Scarp orientation in regions of active aeolian erosion on Mars

Joshua Williams[1,2], Mackenzie Day[3*], Matthew Chojnacki[4], Melissa Rice[1],

[1]Department of Geology, Environmental Studies Building, Western Washington University, 516 High St, Bellingham, WA 98225, USA

[2]Department of Earth and Planetary Sciences, Northrop Hall 141MSC03, University of New Mexico, 221 Yale Blvd. NE, Albuquerque, NM 87131, USA

[3]Department of Earth, Planetary, and Space Sciences, University of California Los Angeles, 595 Charles Young Dr. E., Los Angeles, CA, 90095, USA

[4]Lunar and Planetary Laboratory, University of Arizona, Tucson, AZ 85721, USA

**Corresponding author:* daym@epss.ucla.edu

ABSTRACT

The morphologies of wind-formed features on Mars provide diagnostic information about ancient and modern surface winds. Aeolian erosional features include decimeter-scale ventifacts and kilometer-scale yardangs, but intermediate-scale erosional features are less well-understood. Understanding aeolian erosion may be critical to identifying ancient martian biosignatures. Cosmogenic radiation destroys complex organic molecules during prolonged exposure at the martian surface, but outcrops freshly re-exposed by aeolian erosion provide potential sites where biosignatures could have been protected and made recently available for sampling. Wind-driven scarp retreat has been cited as the cause for young exposure ages measured in Gale crater.

Upcoming exploration by the Mars 2020 rover will focus on Jezero crater, another location of extensive aeolian erosion and meter-scale scarps. This work is motivated by the hypothesis that retreating scarps on Mars may prefer orientations that reflect the direction of erosive winds. We mapped scarps in Jezero and Gale craters and compared their orientation distributions with local wind regimes interpreted from other aeolian indicators. No strong correlation between wind direction and scarp orientation was identified. The near-random distribution of scarp orientations suggests that in the locations studied the dominant processes controlling scarp orientation are either processes that do not prefer an orientation (e.g., impact or thermal fracturing processes), or that turbulent flow structures form at the scale of scarp topography and obscure the regional-scale signals of erosion with scarp-scale eddies and flow deflection.

INTRODUCTION

Aeolian erosion is pervasive on Mars and leaves behind geomorphic signatures that can be used to interpret the local wind regime. Sand entrained by the wind collides with exposed surfaces, causing abrasion and forming characteristic textures of wind-driven erosion at a variety of scales. At the largest scale, wind can carve kilometer-scale yardangs that form fields of parallel ridges tapering toward the downwind direction (Blackwelder, 1934; Ward, 1979). At meter- and centimeter-scales, wind carves flutes and grooves into rock surfaces, forming ventifacts from cobbles and boulders (Sharp, 1949; Bridges et al., 1999, 2014; Knight, 2008; Laity and Bridges, 2009). Intermediate scales of erosion necessarily occur, but can be more difficult to interpret. Decameter aeolian bedforms including dunes (Hayward et al., 2014) and transverse aeolian ridges (Balme et al., 2008) form from a sediment supply that could be used for abrasion, but bedforms are depositional features and do not inherently indicate erosion. Aeolian erosion has been interpreted to form decameter-scale periodic bedrock ridges on Mars (Montgomery et al., 2012; Hugenholtz et al., 2015). These linear features orient normal to the eroding winds, however,

periodic bedrock ridges share morphological characteristics with aeolian bedforms and are not always easy to identify as erosional features in orbital images. Aeolian erosion has been cited as a likely driving mechanism for removing many tens of thousands of cubic kilometers of sediment across Mars (Malin and Edgett, 2000; Schon et al., 2012; Day et al., 2016;), an interpretation commonly based on kilometer-scale geologic context. A decameter- or hundred-meter-scale signature of aeolian erosion reflecting its formative wind direction could significantly improve the precision with which we interpret aeolian erosion on Mars.

Understanding the rates and directions of aeolian erosion can help reconstruct landscape evolution and is critical to the search for preserved signatures of biological activity on Mars. Organic molecules formed by hypothetical martian life would degrade on timescales of a few hundred million years or less when exposed to galactic and solar cosmic rays at the martian surface (Dartnell et al., 2007a,b, Pavlov et al., 2012). Ancient burial could have shielded molecular evidence of ancient life from degradation, and recent aeolian erosion could expose preserved biosignatures to robotic exploration and sampling (Farley et al., 2014; Grotzinger et al., 2015). For this reason, understanding aeolian erosion at the scale of retreating scarps is key to maximizing the likelihood of detecting ancient martian life. Scarps may represent the critical intermediate-scale signatures of aeolian erosion, and in this work we investigate whether scarp orientations can be used as a tool to understand long-term wind regimes and directions of aeolian erosion on Mars.

Scarps form meter-scale topographic steps across Mars and have been suggested to evolve through a combination of aeolian erosion (Ward, 1979), ancient fluvial activity (Milton, 1973) and mass wasting (Hugenholtz, 2008) helped by thermal and impact stresses. In Gale crater, the Mars Science Laboratory team used instruments onboard the rover Curiosity to measure an exposure age of 78 ± 30 Ma below an eroding scarp (Farley et al., 2014). The young exposure age was attributed to

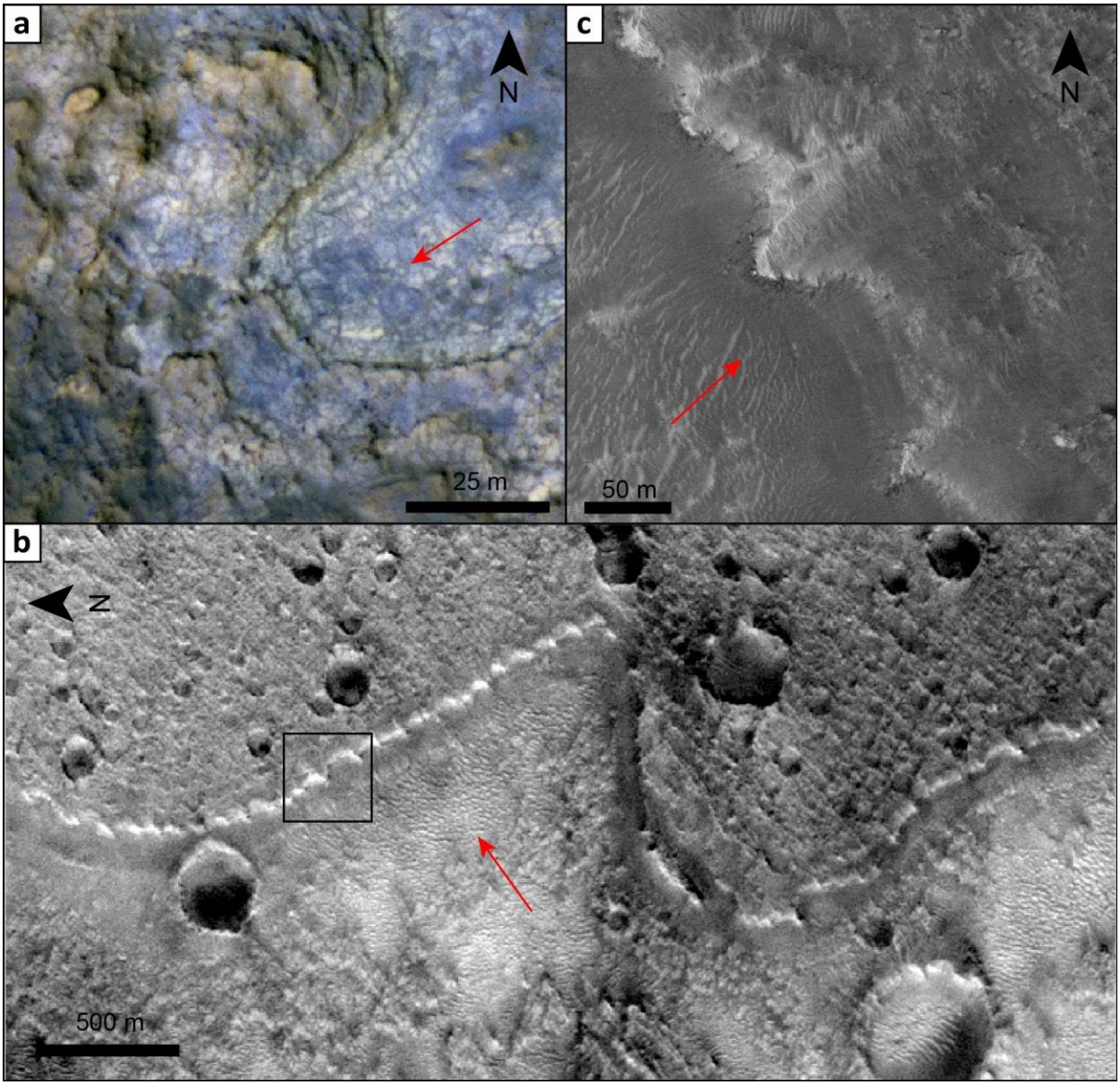

Figure 1: Retreating scarps. a) A retreating scarp in Gale crater near the Cumberland drill location where samples from the Mars Science Laboratory rover led to an estimated exposure age of ~78 Ma. Scarp retreat has been attributed in part to aeolian erosion by northeasterly winds (red arrow). HiRISE image: ESP_040269_1755. b) A retreating scarp in Jezero crater defining the margin of the volcanic floor unit. Scalloping along the edge of the scarp has been interpreted as a proto-yardang texture from southwesterly winds (red arrow). The location of (c) is boxed in black. CTX image P06_003376_1987_XN_18N283W. c) A close-up image of the edge of the volcanic floor unit shows the scarp retreating to form bays opening toward the southwest. Red arrow indicates the interpreted paleo-wind direction. HiRISE image ESP_023524_1985.

aeolian driven erosion of the surrounding scarp, which forms a "U" shape opening toward the upwind direction (termed here as a "bay") interpreted from nearby aeolian features (Fig. 1a; Hobbs et al., 2010; Day and Kocurek, 2015). A similar pattern of upwind facing bays was also identified along the scarped margin of a mafic crater-floor unit in Jezero crater (Goudge et al., 2015; Day and Dorn, 2019). Here, a series of U-shaped scallops open toward the interpreted upwind direction and are not developed when the scarp margin curves parallel to the wind (Fig. 1b). Both Gale and Jezero craters have experienced significant aeolian erosion of their interiors (Fassett and Head, 2005; Schon et al., 2012; Day and Kocurek, 2015), consistent with observed contemporary sand movement (Silvestro et al., 2013; Chojnacki et al., 2018), and the observed erosional bays suggest a possible relationship between scarp orientation and wind direction in regions of active aeolian erosion. In this work, we mapped scarps in Jezero and Gale craters and compared the measured scarp orientations with wind directions interpreted in previous works. Possible outcomes of this comparison include: (1) scarp orientations tend to align normal to the eroding wind direction, indicating scarp faces are blunted and step back uniformly, (2) scarps tend to orient parallel to the eroding wind direction, similar to yardangs and possibly reflecting a preliminary stage before full yardang formation, (3) scarps tend to orient in bimodal distributions of parallel and perpendicular to the winds with the modality of each orientation reflecting the extent of erosion, and (4) scarp orientation does not correlate with wind direction, indicating a different geologic agent controls scarp erosion. A strong alignment of scarp orientations demonstrating (1), (2), or (3) would imply that scarp orientation is significantly influenced by wind and that scarps can be used as a tool to understand local wind regime.

STUDY AREAS

In this work, we take advantage of the body of work surrounding Gale and Jezero craters and use these two crater basins as case studies to test for strong correlations between scarp

orientations and interpreted wind directions. Both Gale and Jezero craters have been interpreted to have once housed ancient crater lakes (Fassett and Head, 2005; Schon et al., 2012; Grotzinger et al., 2014, 2015) and now are both home to layered interior deposits (Anderson and Bell, 2010; Wray, 2013; Goudge et al., 2015). These deposits likely vary between the craters (e.g., in grain size, cementation, composition, or lithologic strength), but both have undergone extensive aeolian erosion. In Gale crater (5.4° N, 137.8° E), the exploration site of the Mars Science Laboratory (MSL) rover Curiosity, the predominating wind regime has been interpreted from the diverse wind-formed surface features, including dunes (Hobbs et al., 2010; Silvestro et al., 2013), ventifacts (Bridges et al., 2014), migrating ripples (Silvestro et al., 2013; Lapotre et al., 2016), streamlined nodules (Sun et al., 2019), and transverse aeolian ridges (Day and Kocurek, 2015). Collectively, these features describe a crater interior in which northerly winds interact with the crater rim and are diverted around the central mound, causing northeasterly winds along the part of the rover traverse studied in this work (Day and Kocurek, 2015). The first study area falls along the rover traverse in Gale crater from sols 1-1500 of the MSL mission, and covers the basal strata of the central sedimentary mound Aeolis Mons, informally known as Mount Sharp (Fig. 2). Although basal lacustrine mudstones (Rampe et al., 2017; Sun et al., 2019) and aeolian sandstones (Banham et al., 2018) suggest ancient Gale crater was at least partially filled and the central mound later eroded to its current morphology by wind (Malin and Edgett, 2000; Day et al., 2016), an alternative explanation for the central mound invokes slope-driven or katabatic winds as a mechanism of deposition (Kite et al., 2013, 2016), in which case, southerly winds coming down from the central mound could have dominated the study area in the past.

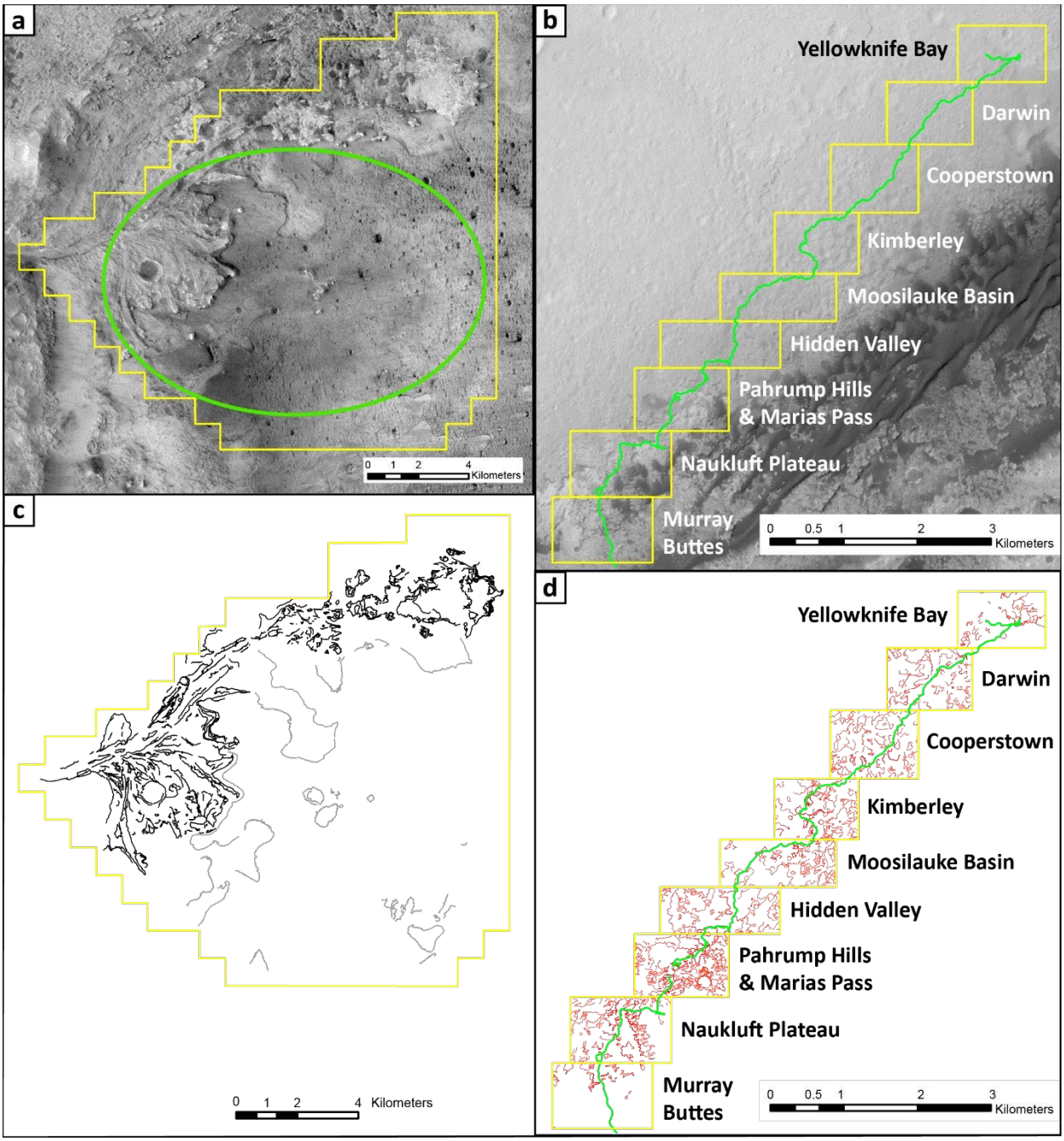

Figure 2: Study areas in Jezero and Gale craters. a) Study area in Jezero crater including the delta deposit and western margin of the crater floor. Yellow lines outline the area inside of which the scarps were mapped. Green indicates the approximate position of the Mars 2020 landing ellipse. b) Study area in Gale crater along the Curiosity rover traverse. Nine subdivisions of the study area (yellow boxes) along the traverse (green line) are named for notable exploration waypoints. Background images in (a) and (b) are CTX image mosaics. c) The scarps mapped in Jezero crater. Crater floor (grey) and delta (black) scarps are morphologically very different and were separated for analysis. d) Scarps mapped in Gale crater (red).

Scarp density varies along the traverse, but is consistently higher in Gale crater than Jezero crater. North is up in all images.

Jezero crater (19° N, 77.5° E) hosts a paleo-delta deposit in its western interior (Fig. 2b) along with mafic units, clay-bearing strata, and carbonate-bearing units in the crater center and margins (Ehlmann et al., 2008; Goudge et al., 2017; Salvatore et al., 2018), and is the planned landing site for the Mars 2020 rover. Isolated exposures of the western delta deposit indicate that ~3 km^3 of material have been eroded from the delta (Goudge et al., 2018), presumably by aeolian erosion (Schon et al., 2012). Long wind streaks and the migration patterns of bedforms describe a modern wind regime dominated by easterly winds in Jezero crater (Chojnacki et al., 2018). Older textures of aeolian erosion, interpreted as proto-yardangs, suggest earlier erosion in Jezero crater may have been perpetrated by southwesterly winds (Day and Dorn, 2019). Further characterization of the local winds will be available after the Mars 2020 rover lands via data from the Mars Environmental Dynamics Analyzer (Rodriguez-Manfredi et al., 2014), but available evidence suggests a history of early southwesterly winds followed by modern easterly winds.

METHODS

Mapping areas were defined over a tractable mapping extent along the Curiosity rover traverse in Gale crater, and to cover the interior of Jezero crater, including the presumptive exploration region for the Mars 2020 rover (Fig. 2a,b). Lithologic variations along the study area in Gale crater are not readily distinguishable in satellite images, but have been studied using surface data (e.g., the Murray mudstone, Rampe et al., 2017; the Bradbury group, Siebach et al., 2017). In Jezero crater, however, the study area covers an easily distinguished ancient delta deposit, and crater-floor volcanic and "mottled" units (Goudge et al., 2015). To investigate the possible effects of lithology on scarp distribution, we separated measurements of the Jezero crater floor and delta deposits to allow for both separate and holistic analysis of measurements (Fig. 2a,c). Within Gale

157 crater, the density of scarps was much higher (Table 1). We divided the traverse into nine sub-
158 regions, each covering 0.5-1.5 km^2, and roughly corresponding with exploration waypoints (Fig.
159 2b). The study area covers the rover traverse from the landing site near Yellowknife Bay to the
160 Murray Buttes, Curiosity's approximate location on sol 1441 (Fig. 2d).
161 Scarp density was nonuniform along the traverse and is presented both separately for each
162 measured region and combined in Table 1. Mapping scarps in the vicinity of the rover traverse also
163 allowed us to verify that scarps mapped in images taken from orbit were also visible as scarps at
164 the surface. See supplementary material for additional verification methods.
165 Mapping was performed in ArcGIS by tracing scarps in high resolution images from the
166 High Resolution Imaging Science Experiment. (HiRISE; ~ 25 cm/px; McEwen et al., 2007)
167 onboard the Mars Reconnaissance Orbiter. Continuous HiRISE imaging coverage is available
168 across all mapped areas. By definition, scarps form a step in topography separating one low and
169 one high surface. To preserve the directionality of scarps with respect to the low and high sides of
170 the scarp trace, we establish a right-hand-rule as follows: all scarp orientations are presented so
171 that someone facing toward the stated direction would have the high elevation side of the scarp
172 step on their right. Mapping practices and the reported scarp orientations follow this rule.
173 Scarp azimuth orientations were calculated from the end points of linear segments of the
174 scarp trace and weighted by the segment length. The orientations plotted in Figure 4 and values
175 presented in Table 1 reflect the frequency per meter of scarp. Scarp density was defined as the
176 combined lengths of measured scarps divided by the area over which they were measured. To
177 quantify the spread of the measured orientations, we calculated the mean resultant length, R, a
178 summary statistic for circular data that varies from one for perfectly aligned data to zero for
179 uniformly distributed data (Fisher, 1993). Note that the mean resultant length is related to the
180 summary statistic of circular variance, V, as V = 1-R (Harrison et al., 1986). The goal of this work

was to determine whether scarp orientations prefer any particular orientation and how that orientation related to the wind. The wind directions driving erosion in Jezero and Gale craters have been the subject of previous literature (Bridges et al., 2014; Day et al., 2016; Chojnacki et al., 2018; Day and Dorn, 2019) and are discussed in the previous section. Rather than re-analyzing features in our study sites, we refer to the previously interpreted wind regimes (red arrows in Fig. 1) for comparison with scarp orientation results and interpret that any strong clustering of orientations likely reflects a unidirectional forcing (most likely wind).

Table 1: Scarp measurement summary for regions in Gale crater and Jezero crater. R is the mean resultant length, a statistical measure of the angular spread varying from 1 (no spread) to 0 (uniform spread).

	Study area	Area mapped (km^2)	Scarps mapped (m)	Scarp density (m/km^2)	R
Gale	Yellowknife Bay	0.85	7,383	8,686	7×10^{-4}
	Darwin	1.01	13,915	13,777	1×10^{-3}
	Cooperstown	1.11	18,141	16,344	8×10^{-4}
	Kimberley	0.93	16,090	17,301	7×10^{-4}
	Moosilauke Basin	0.97	15,182	15,652	8×10^{-4}
	Hidden Valley	1.08	16,818	15,572	3×10^{-4}
	Pahrump Hills and Marias Pass	1.15	29,852	25,958	2×10^{-4}
	Naukluft Plateau	1.07	18,616	17,398	1×10^{-3}
	Murray Buttes	1.34	6,380	4,761	9×10^{-4}
	Total	**9.51**	142,377	14,971	6×10^{-5}
Jezero	Delta deposit	56	291,653	5,208	4×10^{-5}
	Crater floor units	94	67,382	717	1×10^{-4}
	Total	**150**	359,035	2,394	3×10^{-5}

RESULTS

The quantitative measurements made in this work are summarized in Table 1.

194 In Gale crater, a total of 142,377 m of scarps were mapped in 9.51 km^2 along the Curiosity
195 rover traverse. Collectively the nine study areas had a total scarp density of 14,971 m/km^2. The
196 Pahrump Hills and Marias Pass region had the highest scarp density of any individual quadrangle
197 (29,852 m/km^2) and the Murray Buttes region had the lowest density (6,380 m/km^2). The combined
198 R-value of scarp orientation distribution in Gale crater was 6 x 10^{-5}, indicating a very low level of

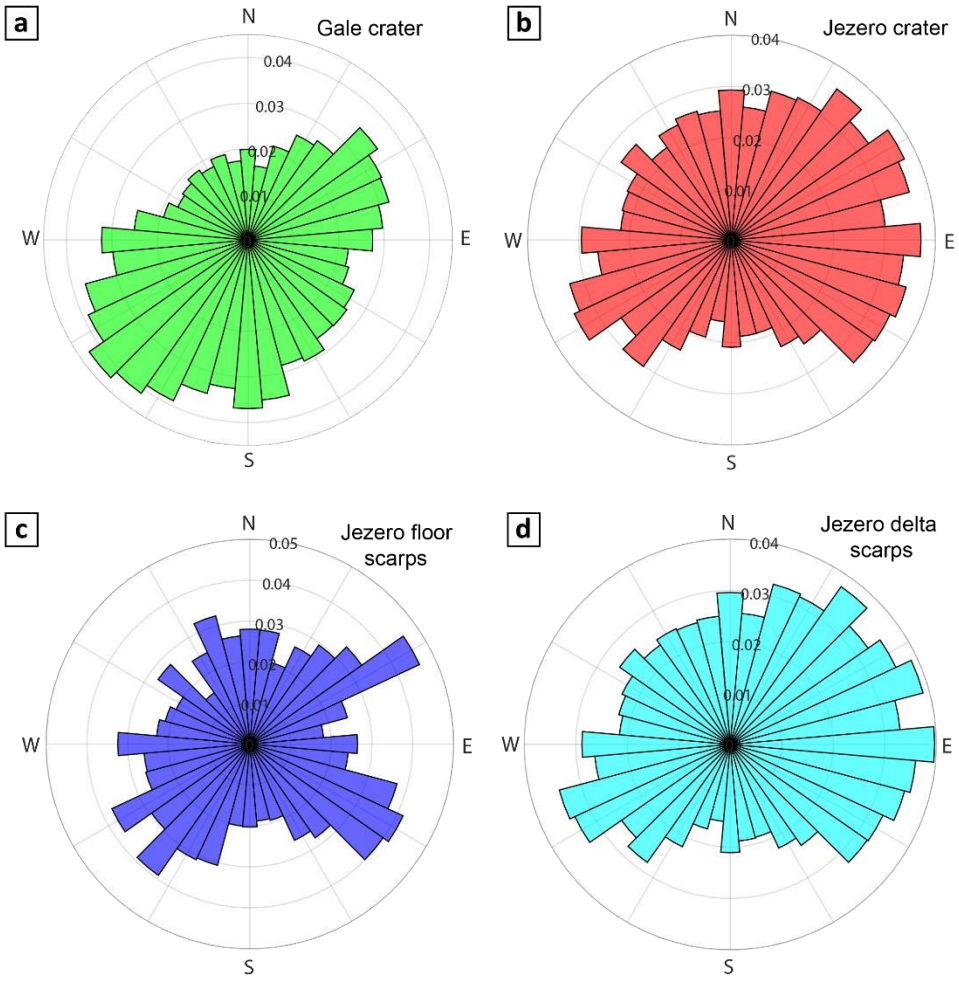

199

200 **Figure 3:** Distributions of measured scarp orientations. a) Scarps measured in the study area of Gale crater,
201 a combined area of 9.5 km^2 (Table 1). b) Scarps measured in the Jezero crater study area (150 km^2). c)
202 Scarps measured on the floor of Jezero crater, primarily defining the margin of the volcanic floor unit of
203 Goudge et al. (2015). d) Scarps mapped on the Jezero delta deposits. Sample sizes are given in Table 1.
204

ordering approaching a uniform radial distribution. To test possible lateral variations or local coincidence with wind regime, R values were calculated for each of the nine study areas separately (Table 1). In no case was the calculated R value >0.01.

In Jezero crater, a total of 359,035 m of scarps were mapped in an area of 150 km^2 (Fig. 2). Subdividing this into the delta deposit (56 km^2) and crater floor units (94 km^2), 291,653 m and 67,382 m of scarps were mapped, respectively. The density of scarp exposures in Jezero crater varied significantly between the delta (5,208 m/km^2) and crater floor (717 m/km^2), and is presumably attributable to the difference in lithology and possibly unit age. As in Gale crater, the mean resultant statistic R was always low, indicating no ordering in any particular direction (Fig. 3). In Jezero crater for each subdivision (i.e., delta deposit, crater floor, and combined) R was always <0.001 (Table 1).

DISCUSSION

Despite the robust geomorphological indicators of long-lived, erosive surface winds in Jezero and Gale craters, the orientations of scarps in each location do not prefer any particular direction, let alone one corresponding to the direction of the wind. For all subdivisions of the measured areas, scarp orientations do not significantly deviate from random distributions. Assuming aeolian erosion is indeed active in these areas, three explanations could account for the lack of a robust correlation with wind direction (A, B, and C below).

(A) It is possible that the scale of mapping (meter-scale scarp segments) is too coarse or too fine to capture the erosional signal of winds at these locations. Scarps in both Gale and Jezero craters may, over geologic time, evolve to reflect the wind, possibly forming into fields of yardangs or periodic bedrock ridges, but at this stage of development the signal of aeolian erosion may not be present at the mapping scale. Scalloping in Figure 1 clearly shows an erosional texture

developing along a scarp in Jezero crater, however, the scarp has not yet developed enough elongation in the direction of erosion to be reflected in mapping.

(B) The lack of correlation with any one wind regime could have been caused by overprinted signals from multiple wind regimes. For example, in Jezero crater, where both easterly and southwesterly winds have been interpreted for two different time periods (Chojnacki et al., 2018; Day and Dorn, 2019), erosion from one wind regime might have reworked surface textures formed by another wind regime. Depending on the time scales of each period of erosion, scarp orientations might reflect this reworking and superimposed signals from two or more erosive winds might appear similar to a random distribution. In Gale crater, dunes and yardangs suggest northeasterly winds dominate the study area (Silvestro et al., 2013; Day and Kocurek, 2015), but hypothesized slope-driven winds (Kite et al., 2013) could have occurred earlier in the evolution of the crater interior, possibly influencing scarp retreat and obscuring the modern signal.

So far, we have assumed that wind regimes can be represented as unidirectional and that for complex wind regimes scarp erosion would respond on average to a single wind resultant (as is true of dunes; see review in Gao et al. (2015)). Scarps necessarily represent a step in topography, and interactions between airflow and the scarp itself generate turbulence and flow structures that may locally cause abrasion in complex or unexpected geometries. Even where the regional flows are unidirectional, complex interactions between wind and the terrain may cause a locally very different wind regime, causing erosion and scarp retreat to be dominantly controlled by small variations in topography rather than the regional directionality. In Gale crater, the orientations of transverse aeolian ridges are highly variable and presumed to reflect topographic funneling of wind around decameter-scale obstacles (Day and Kocurek, 2015). Scarps form at a similar spatial scale as transverse aeolian ridges and are similarly associated with topographic relief. Aeolian erosion rates depend on angles of incidence between the winds and outcrop (Bridges et al., 2004; 2005)

and the competency of the bedrock (Greeley et al., 1982). Turbulent eddies and other flow structures would complicate these incidence angles, potentially eliminating any signal of directionality with turbulent vorticity (Shao, 2008; Kok et al., 2012). In addition to erosion by direct abrasion, undercutting of competent caprock could cause the caprock to collapse, further speeding erosion, but not necessarily matching the wind direction.

(C) It is also possible that aeolian erosion is not the dominant control on scarp orientation in the study areas. Aeolian erosion is a slow process with estimated rates of abrasion on Mars ranging from nanometers per year (Golombek and Bridges, 2000), to a few microns per year (Farley et al., 2014), to more than ten microns per year (Armstrong and Leovy, 2005; Chojnacki et al., 2018), depending on the location and conditions studied. Regardless of the specific rate, aeolian erosion causes persistent small-magnitude changes over long timescales. In contrast, impacts, thermal stresses, and mass wasting cause high magnitude changes over short timescales. Impact craters tend to create scarps with a radial distribution of orientations instantaneously over geologic time. If craters were the dominant control on scarp formation, the expected distribution would not prefer any single orientation, similar to what was observed in this study. Thermal stresses also act independent of direction and might contribute a random signal to the evolving scarp orientation distribution. Mass wasting, aided by fracturing and aeolian undercutting of caprock, could move large boulders from the tops of steep scarps and may be responsible for a major fraction of scarp retreat and evolution. Mass wasting requires some relief and the cooperation of another mechanism of erosion, but mass wasting itself should not occur preferentially in any one direction.

Differences in lithology also contribute to the development of scarps. Where lithologies vary, the dominant control on scarp formation and evolution may be the original geologic context, mechanical rock strength, or bedding geometry. In Gale crater, the studied area covers a range of

lithologies including mudstone (Rampe et al., 2017), conglomerate (Williams et al., 2013), and sandstone (Banham et al., 2018). Laminations, bedding, or other internal structures could accentuate a particular direction of scarp formation. In Jezero crater, lithologic variability is evident between the delta deposit and crater floor from the differences in weathering pattern.

Scarps form between these, but even within the delta deposit, lithologic heterogeneity is likely present and caused by a variety of fluvio-lacustrine facies. Differing lithologies have different resistances to erosion, and aeolian erosion may have preferentially removed less indurated units on the delta, leading to morphological enhancement of and apparent scarp formation along the existing sedimentary structures. If this were the case, the measured scarp orientations might be expected to align east-west with the progradation direction of the delta, however, the sinuous meandering channels and bar deposits on the delta top could account for a random or radially symmetric distribution of orientations.

CONCLUSIONS

Aeolian erosion has shaped the surface of Mars as evidenced by yardangs, ventifacts, periodic bedrock ridges, and surface textures of erosion. Each of these features reflects in its orientation the direction of its formative winds. Given the abundant evidence of aeolian erosion on Mars, it is presumed that wind plays an important role in scarp erosion, and this study was motivated by the possibility that wind-driven erosion might lead to the preferential orientations in retreating scarps related to the eroding wind direction. Meter-scale measurements of scarps in Gale and Jezero craters returned distributions of scarp orientations with no strong alignment in any direction and bearing no correspondence with the wind directions elsewhere interpreted for these regions from long- and short-term indicators. We conclude that, even where long-term aeolian erosion has taken place, scarp orientations do not reflect a particular wind direction. This suggests that aeolian erosion is either not the dominant control on scarp evolution, that it acts similarly in

multiple directions, or a combination of both. In the first case, impact cratering represents one mechanism that could initiate scarps and would generate a radial (random) distribution of scarp orientations. In the second case, at the meter-scales studied, wind directions and erosion may be dominantly controlled by local topography, including the scarps themselves, leading erosion to be driven by turbulent fluctuations not reflected in interpretations of the dominant overall wind direction. If turbulent fluctuations are the driving force behind erosion, then erosion at all orientations might be expected when eddies and other turbulent flow structures form from largescale flow interacting with scarp-scale topography. Regardless of the mechanism, rover observations demonstrate that wind-driven erosion is pervasive at the surface, but unlike with yardangs and ventifacts, the direction of eroding winds cannot be interpreted from the orientation of meter-scale scarps.

ACKNOWLEDGMENTS

This manuscript greatly benefited from discussions with the late Dr. Nathan Bridges. We also thank Drs. R. Sletten, B. Hallet, D. Clark, B. Foreman, and two anonymous reviewers for their input. G. Speth and J. Dudek assisted with ArcGIS and Python scripting, respectively. We thank J. Zimbleman and three anonymous reviewers for comments that improved this work. J. Williams and M. Rice were supported in part by the NASA Mars Science Laboratory Participating Scientist Program. J. Williams also received support from Western Washington University, and a NASA Mars Program Office student travel grant to attend the Third 2020 Mars Rover Landing Site Workshop. M. Chojnacki was supported by NASA MDAP Grants NNH14ZDA001N.

REFERENCES CITED

Anderson, R., and Bell, J. (2010). Geologic mapping and characterization of Gale Crater and implications for its potential as a Mars Science Laboratory landing site. The Mars Journal, 5, 76–128. https://doi.org/10.1555/mars.2010.0004

Armstrong, J. C., and Leovy, C. B. (2005). Long term wind erosion on Mars. Icarus, 176(1), 57–74. https://doi.org/10.1016/j.icarus.2005.01.005

Balme, M., Berman, D. C., Bourke, M. C., and Zimbelman, J. R. (2008). Transverse Aeolian Ridges (TARs) on Mars. Geomorphology, 101(4), 703–720. https://doi.org/10.1016/j.geomorph.2008.03.011

Banham, S. G., Gupta, S., Rubin, D. M., Watkins, J. A., Sumner, D. Y., Edgett, K. S., et al. (2018). Ancient Martian aeolian processes and palaeomorphology reconstructed from the Stimson formation on the lower slope of Aeolis Mons, Gale crater, Mars. Sedimentology. DOI:10.1111/sed.12469. https://doi.org/10.1111/sed.12469

Blackwelder, E. (1934). Yardangs. Geological Society of America Bulletin, 45(1), 159–166.

Bridges, N.T., R. Greeley, A. F. C. Haldemann, K. E. Herkenhoff, M. Kraft, T. J. Parker, A. W. Ward (1999) Ventifacts at the Pathfinder landing site. J. Geophys. Res., 104, E4, 8595-8615.

Bridges, N. T., Laity, J. E., Greeley, R., Phoreman, J., and Eddlemon, E. E. (2004). Insights on rock abrasion and ventifact formation from laboratory and field analog studies with applications to Mars. Planetary and Space Science, 52(1), 199–213. https://doi.org/10.1016/j.pss.2003.08.026

Bridges, N., Phoreman, J., White, B. R., Greeley, R., Eddlemon, E. E., Wilson, G. R., and Meyer, C. J. (2005). Trajectories and energy transfer of saltating particles onto rock surfaces: Application to abrasion and ventifact formation on Earth and Mars. Journal of Geophysical Research - Planets, 110(E12), E12004. https://doi.org/10.1029/2004je002388

Bridges, N., Kocurek, G. A., Langevin, Y., Lewis, K. W., Mangold, N., Maurice, S., et al. (2014). The rock abrasion record at Gale Crater: Mars Science Laboratory results from Bradbury Landing to Rocknest. Journal of Geophysical Research - Planets, 119(6), 1374–1389. https://doi.org/10.1002/2013je004579

Chojnacki, M., Banks, M., and Urso, A. (2018). Wind-Driven Erosion and Exposure Potential at Mars 2020 Rover Candidate-Landing Sites. Journal of Geophysical Research: Planets, 123(2), 468–488.

Dartnell, L. R., L. Desorgher, J. M. Ward, and A. J. Coates (2007a), Martian sub-surface ionising radiation: biosignatures and geology, Biogeosciences Discussions, 4(1), 455–492.

Dartnell, L. R., L. Desorgher, J. M. Ward, and A. J. Coates (2007b), Modelling the surface and subsurface Martian radiation environment: Implications for astrobiology, Geophysical Research Letters, 34(2). doi:10.1029/2006GL027494

Day, M., and Dorn, T. (2019). Wind in Jezero crater, Mars. Geophysical Research Letters, 46. https://doi.org/10.1029/2019GL082218

Day, M., and Kocurek, G. (2015). Observations of an aeolian landscape: From surface to orbit in Gale Crater. Icarus. https://doi.org/10.1016/j.icarus.2015.09.042

Day, M., Anderson, W., Kocurek, G., and Mohrig, D. (2016). Carving intra-crater layered deposits with wind on Mars. Geophysical Research Letters, 43(6), 2473-2479.

Ehlmann, B. L., Mustard, J. F., Fassett, C. I., Schon, S. C., Head III, J. W., Marais, D. J. Des, et al. (2008). Clay minerals in delta deposits and organic preservation potential on Mars. Nature Geoscience, 1(6), 355–358.

Farley, K. A., Hurowitz, J. A., Grant, J. A., Miller, H. B., Arvidson, R., Beegle, L., et al. (2014). In situ radiometric and exposure age dating of the martian surface. Science, 343(6169), 1247166. https://doi.org/10.1126/science.1247166

Fassett, C. I., and Head, J. W. (2005). Fluvial sedimentary deposits on Mars: Ancient deltas in a crater lake in the Nili Fossae region. Geophysical Research Letters, 32(14).

Fisher, N. I. (1993). Statistical analysis of circular data. New York: Cambridge University Press.

Gao, X., Narteau, C., Rozier, O., and du Pont, S. C. (2015). Phase diagrams of dune shape and orientation depending on sand availability. Scientific Reports, 5, 14677. https://doi.org/10.1038/srep14677

Golombek, M. P., and Bridges, N. T. (2000). Erosion rates on Mars and implications for climate change: Constraints from the Pathfinder landing site. Journal of Geophysical ResearchPlanets, 105(E1), 1841–1853.

Goudge, T. A., Mustard, J. F., Head, J. W., Fassett, C. I., and Wiseman, S. M. (2015). Assessing the mineralogy of the watershed and fan deposits of the Jezero crater paleolake system, Mars. Journal of Geophysical Research: Planets, 120(4), 775–808.

Goudge, T. A., Milliken, R. E., Head, J. W., Mustard, J. F., & Fassett, C. I. (2017). Sedimentological evidence for a deltaic origin of the western fan deposit in Jezero crater, Mars and implications for future exploration. *Earth and Planetary Science Letters*, *458*, 357–365.

Goudge, T. A., Mohrig, D., Cardenas, B. T., Hughes, C. M., and Fassett, C. I. (2018). Stratigraphy and paleohydrology of delta channel deposits, Jezero crater, Mars. Icarus, 301, 58–75.

Greeley, R., R. N. Leach, S. H. Williams, B. R White, J. B. Pollack, S. H. Krinsley, J. R. Marshall (1982) Rate of wind abrasion on Mars. J. Geophys. Res., 87, 10009-10024.

Grotzinger, J. P., Mangold, N., Milliken, R., Conrad, P. G., DesMarais, D., Farmer, J., et al. (2014). A habitable fluvio-lacustrine environment at Yellowknife Bay, Gale crater, Mars. Science, 343(6169), 1242777. https://doi.org/10.1126/science.1242777

Grotzinger, J. P., Gupta, S., Malin, M. C., Rubin, D. M., Schieber, J., Siebach, K., et al. (2015). Deposition, exhumation, and paleoclimate of an ancient lake deposit, Gale crater, Mars. Science, 350(6257), aac7575-U69. https://doi.org/10.1126/science.aac7575

Harrison, D., Kanji, G. K., & Gadsden, R. J. (1986). Analysis of variance for circular data. *Journal of Applied Statistics*, *13*(2), 123–138.

Hayward, R. K., Fenton, L. K., and Titus, T. N. (2014). Mars Global Digital Dune Database (MGD(3)): Global dune distribution and wind pattern observations. Icarus, 230, 38–46. https://doi.org/10.1016/j.icarus.2013.04.011

Hobbs, S. W., Paull, D. J., and Bourke, M. C. (2010). Aeolian processes and dune morphology in Gale Crater. Icarus, 210(1), 102–115.

Hugenholtz, C. H. (2008). Frosted granular flow: A new hypothesis for mass wasting in martian gullies. *Icarus*, *197*(1), 65–72.

Hugenholtz, C. H., Barchyn, T. E., and Favaro, E. A. (2015). Formation of periodic bedrock ridges on Earth. Aeolian Research, 18, 135–144.

Kite, E. S., Lewis, K. W., Lamb, M. P., Newman, C. E., and Richardson, M. I. (2013). Growth and form of the mound in Gale Crater, Mars: Slope wind enhanced erosion and transport. Geology, 41(5), 543–546. https://doi.org/10.1130/g33909.1

Kite, E. S., Sneed, J., Mayer, D. P., Lewis, K. W., Michaels, T. I., Hore, A., and Rafkin, S. C. R. (2016). Evolution of major sedimentary mounds on Mars: Buildup via anticompensational stacking modulated by climate change. Journal of Geophysical Research: Planets, 121(11), 2282–2324.

Knight, J. (2008) The environmental significance of ventifacts: A critical review. Earth Sci. Rev., 86, 89-105.

415 Kok, J. F., Parteli, E. J. R., Michaels, T. I., and Karam, D. B. (2012). The physics of wind-blown
416 sand and dust. Reports on Progress in Physics. Physical Society (Great Britain), 75(10),
417 106901. https://doi.org/10.1088/0034-4885/75/10/106901
418 Laity, J. E., N. T. Bridges (2009) Ventifacts on Earth and Mars: Analytical, field and laboratory
419 studies supporting sand abrasion and windward feature development. Geomorph., 105(3-4),
420 202-217.
421 Lapotre, M. G. A., Ewing, R. C., Lamb, M. P., Fischer, W. W., Grotzinger, J. P., Rubin, D. M., et
422 al. (2016). Large wind ripples on Mars: A record of atmospheric evolution. Science,
423 353(6294), 55–58. https://doi.org/10.1126/science.aaf3206
424 Malin, M. C., and Edgett, K. S. (2000). Sedimentary rocks of early Mars. Science, 290(5498),
425 1927–1937.
426 McEwen, A. S., Eliason, E. M., Bergstrom, J. W., Bridges, N. T., Hansen, C. J., Delamere, W.
427 A., et al. (2007). Mars Reconnaissance Orbiter's High Resolution Imaging Science
428 Experiment (HiRISE). Journal of Geophysical Research: Planets, 112(E5).
429 https://doi.org/10.1029/2005je002605
430 Milton, D. J. (1973). Water and processes of degradation in the Martian landscape. Journal of
431 Geophysical Research, 78(20), 4037–4047.
432 Montgomery, D. R., Bandfield, J. L., and Becker, S. K. (2012). Periodic bedrock ridges on Mars.
433 Journal of Geophysical Research: Planets, 117(E3). https://doi.org/10.1029/2011je003970
434 Pavlov, A. A., Vasilyev, G., Ostryakov, V. M., Pavlov, A. K., and Mahaffy, P. (2012). Degradation
435 of the organic molecules in the shallow subsurface of Mars due to irradiation by cosmic rays.
436 Geophysical Research Letters, 39(13). https://doi.org/10.1029/2012gl052166
437 Rampe, E. B., Ming, D. W., Blake, D. F., Bristow, T. F., Chipera, S. J., Grotzinger, J. P., et al.
438 (2017). Mineralogy of an ancient lacustrine mudstone succession from the Murray formation,
439 Gale crater, Mars. Earth and Planetary Science Letters, 471, 172–185.
440 Rodriguez-Manfredi, J. A., de la Torre, M., Conrad, P., Lemmon, M., Martinez, G., Newman, C.,
441 et al. (2014). MEDA: an environmental and meteorological package for Mars 2020. 45th
442 Lunar and Planetary Science Conference, abstract 2837. Woodlands, TX.
443 Salvatore, M. R., Goudge, T. A., Bramble, M. S., Edwards, C. S., Bandfield, J. L., Amador, E.
444 S., et al. (2018). Bulk mineralogy of the NE Syrtis and Jezero crater regions of Mars derived
445 through thermal infrared spectral analyses. Icarus, 301, 76–96.
446 Schon, S. C., Head, J. W., and Fassett, C. I. (2012). An overfilled lacustrine system and
447 progradational delta in Jezero crater, Mars: Implications for Noachian climate. Planetary and
448 Space Science, 67(1), 28–45.
449 Shao, Y. (2008). Physics and modelling of wind erosion (Vol. 37). Springer Science and Business
450 Media.
451 Sharp, R. P. (1949) Pleistocene ventifacts east of the Big Horn Mountains, Wyoming. J. Geology,
452 57(2), 175-195.
453 Siebach, K. L., Baker, M. B., Grotzinger, J. P., McLennan, S. M., Gellert, R., Thompson, L. M.,
454 and Hurowitz, J. A. (2017). Sorting out compositional trends in sedimentary rocks of the
455 Bradbury group (Aeolis Palus), Gale crater, Mars. Journal of Geophysical Research: Planets,
456 122(2), 295–328.
457 Silvestro, S., Vaz, D. A., Ewing, R. C., Rossi, A. P., Fenton, L. K., Michaels, T. I., et al. (2013).
458 Pervasive aeolian activity along rover Curiosity's traverse in Gale Crater, Mars. Geology,
459 41(4), 483–486. https://doi.org/10.1130/g34162.1

460 Sun, V. Z., Stack, K. M., Kah, L. C., Thompson, L., Fischer, W., Williams, A. J., et al. (2019).
461 Late-stage diagenetic concretions in the Murray formation, Gale crater, Mars. Icarus, 321,
462 866–890. https://doi.org/https://doi.org/10.1016/j.icarus.2018.12.030
463 Ward, A. W. (1979). Yardangs on Mars - Evidence of recent wind erosion. Journal of
464 Geophysical Research, 84(B14), 8147–8166. https://doi.org/10.1029/JB084iB14p08147
465 Williams, R. M. E., Maurice, S., Forni, O., Gasnault, O., Ollila, A., Newsom, H. E., et al. (2013).
466 Martian Fluvial Conglomerates at Gale Crater. Science, 340(6136), 1068–1072.
467 https://doi.org/10.1126/science.1237317
468 Wray, J. J. (2013). Gale crater: the Mars Science Laboratory/Curiosity Rover Landing Site.
469 International Journal of Astrobiology, 12(1), 25–38.
470 https://doi.org/10.1017/s1473550412000328

Scarp orientation in regions of active aeolian erosion on Mars

Joshua Williams[1,2], Mackenzie Day[3*], Matthew Chojnacki[4], Melissa Rice[1],

SUPPLEMENTARY MATERIAL

Mapping methods

As topographic steps, scarps cast shadows and highlight unit boundaries, making them easy to identify in images taken from orbit using a combination of shadows and textural differences. Scarps that were obscured by unconsolidated sediment (e.g., mantling or bedforms) or were less than 50 m in length were not mapped. Parallel scarps spaced within 10 m that had the same orientation (e.g., forming steps rather than a valley) were mapped as a single scarp. Differences in solar illumination angle across adjacent images were assumed not to inhibit the identification of scarps. To confirm this, we created several shaded relief maps from a HiRISE digital terrain model (DTM) covering the Pahrump Hills and Marias Pass section of the study area (Fig. 2; main text). Scarps were re-mapped in shaded relief maps with different illuminations and all scarps initially mapped in HiRISE images were identifiable under the different simulated illumination geometries tested (Fig. S1).

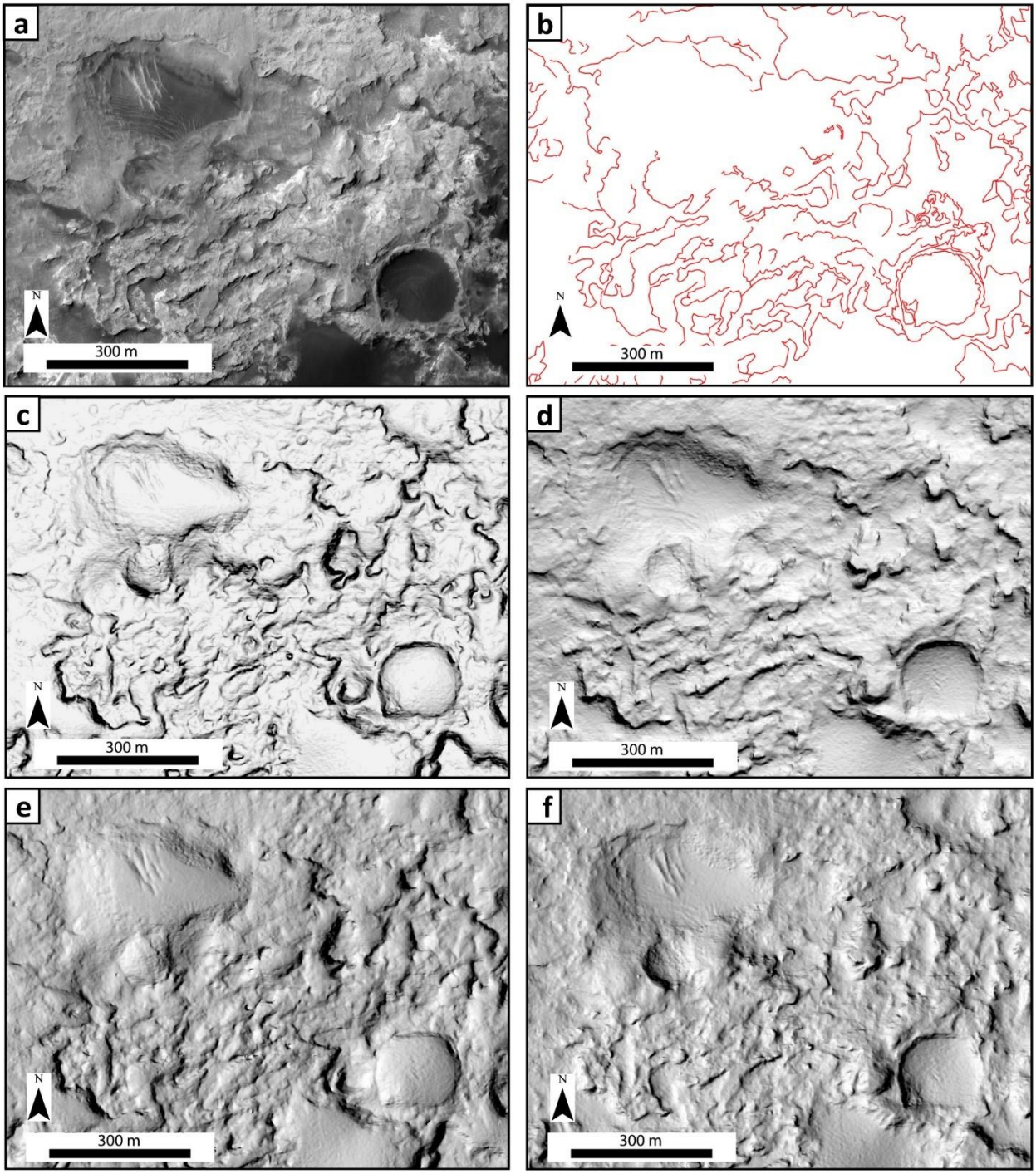

Figure S1: Test of the effects of illumination angle on scarp mapping results for the Pahrump Hills and Marias Pass quadrangle. a) HiRISE image ESP_018920_1755; b) scarps as mapped using the HiRISE image; c-f) shaded relief maps created from HiRISE DTM DTEEC_018854_1755_018920_1755_U01 with varying solar illumination angles: c) elevation 90°; d) elevation 70°, azimuth 0°; e) elevation 70°, azimuth 90°; f)

elevation 70°, azimuth 270°. The scarps mapped in (b) are identifiable in each of the simulated solar illumination scenarios, even with the Sun directly overhead as modeled in (c).